Coupling spectral and Finite Element methods for 3D physic-based seismic analysis from fault to structure: Application to the Cadarache site in France

Reine Fares, David Alejandro Castro Cruz, Evelyne Foerster, Fernando Lopez-caballero, Filippo Gatti

Coupling Spectral and Finite Element Methods for 3D physic-based seismic analysis from fault to structure: application to the Cadarache site in France

Reine Fares[1,2*], David Castro Cruz[3], Evelyne Foerster[2], Fernando Lopez-Caballero[3], Filippo Gatti[3]

[1] Université Paris-Saclay, CEA, Service d'Études Mécaniques et Thermiques, 91191, Gif-sur-Yvette, France.

[2] Université Paris-Saclay, CEA, Département de Modélisation des Systèmes et Structures, 91191, Gif-sur-Yvette, France.

[3] Université Paris-Saclay, CentraleSupélec, ENS Paris-Saclay, CNRS, Laboratoire de Mécanique Paris-Saclay, 91190, Gif-sur-Yvette, France.

Corresponding author:

Reine Fares

Laboratoire d'Etudes Mécaniques Sismiques

CEA/DES/ISAS/DM2S/SEMT/EMSI

Address: CEA SACLAY - Bât 603, 91191 Gif Sur Yvette Cedex, France

Email: reine.fares@cea.fr

Mobile: 0033666413907

Abstract

This paper presents the application of a coupling strategy between the Spectral (SEM) and Finite Element (FEM) Methods to solve the soil-structure interaction (SSI) problem. The SEM-FEM coupling benefits from the mesh refinement capabilities of the FEM in modeling the structure and the near soil, with the realism of the SEM for regional scale earthquake simulations from the fault to the site. To this end, the Domain Reduction Method (DRM) introduced by (Bielak et al., 2003) is herein employed. The DRM formulation solves the problem of multi-scale earthquake simulations by subdividing the fault-to-structure problem into two simpler ones, namely: problem I- containing the structure and (hereafter solved using the FEM) and problem II- containing the fault, the regional geological and surface topography, the sedimentary basin (hereafter solved using the SEM). In this work, the coupling between the FEM code CAST3M and the SEM code SEM3D is presented, verified and compared to conventional 1D deconvolution methods for SSI analysis. A seismic simulation is performed, considering a simplified virtual nuclear reactor building, artificially positioned on the Cadarache site in South-Eastern France. The applicability of the SEM3D-CAST3M coupling is demonstrated, for SSI analysis in linear elastic regime and with a 50% reduction of the model dimensions. Moreover, the coupling captures the amplified response for the nuclear structure due to the 3D spatially variable input field and to the resulting surface wave propagation in the SEM-FEM SSI analysis.

Keywords: Nuclear reactor building; Soil-structure interaction; seismic analysis; weak coupling; Finite Element Method; Spectral Element Method.

1. INTRODUCTION

In recent years, a continuous effort to establish improved earthquake engineering modeling techniques has been made, in order to improve the constitutive behavior models, to characterize the geotechnical and material parameters at stake, to model the site effects and the soil-structure interaction (SSI) with efficient boundary conditions.

One of the largest effort aims at developing more efficient numerical tools to render the complexity of wave propagation phenomena in the Earth's crust and its interaction with the built environment. Despite being the most commonly used tool for earthquake engineering applications (e.g. Fares et al., 2019; Lysmer et al., 1975; Santisi d'Avila and Lenti, 2012), the classical Finite Element Method (FEM) is rarely used for large-scale three-dimensional (3D) seismic wave propagation analyses, due to the high number of integration points per minimum wavelength, with consequent high computation costs and high performance strategies are to be used in this case (e.g. Dupros et al., 2010). Regarding nonlinear large-scale FEM simulations, Ichimura et al., (2014) computed the seismic response of a $2\text{km} \times 2\text{km} \times 0.1\text{km}$ domain representative of a city with $13{,}275$ structures using 10.7 billion degrees of freedom (DOF). On the contrary, methods such as the Spectral Element Method (SEM) (Faccioli et al., 1997; Komatitsch and Vilotte, 1998; Mercerat et al., 2006; Guidotti et al., 2012; Gatti et al., 2018) or the Finite Difference Method (FDM) (e.g. Boore, 1972; Virieux, 1986; Moczo et al., 2004; Maeda et al., 2017) are more popular for seismological and geophysical studies, due to their high accuracy and convenience for parallel implementation.

There are many possible approaches to take into account the SSI and the validity of these approaches strongly depends on the considered assumptions. Following the Niigataken-Chuetsu-Oki earthquake of July 16$^{\text{th}}$ 2007 in Japan, several studies investigated the applied methodologies for SSI analysis (IAEA, 2011, 2009; Wang and Rambach, 2013). Since then, efforts have been made to propose methodologies for seismic design and beyond-design bases of nuclear facilities (Coleman et al., 2013, 2016; Lo Frano et al., 2010; Van Nguyen et al., 2020). Still, at present, the site topography, soil properties, spatial heterogeneity, fault front, and geometry of sedimentary site are neglected and often considered in the signal motion proposed for the site based on nuclear norms recommendations. Hence, the influence of site effects is considered indirectly in assessing seismic ground motions at sites of interest and directly in the modeling of soil horizontally homogeneous stratigraphy. However, studies have shown that the geometry and characterization of the sedimentary basin have a crucial effect on the seismic response (Manakou et al., 2010; Raptakis et al., 2000; Semblat et al., 2005). Koufoudi et al., 2015 investigated the spatial variation of the seismic motion at the ground surface, for the same seismic event, and registered differences in recordings of $15m$ apart. This variation can significantly modify the internal forces induced in the structures (Santisi d'Avila et al., 2022; Sextos and Kappos, 2008). On the other hand, Wang and Feau (2017) investigated the impact of the choice of the control point for the input motion on the SSI in a fragility analysis using a reduced model. The obtained results recommend defining the input at the outcrop for conventional SSI analysis, contrary to the French nuclear authorities recommendations to define the input motion at the free field (FF) (Gupta and Lacoste, 2006).

In order to model the earthquake phenomenon at large scale, from the fault to the structural components, there are few examples of end-to-end simulations (McCallen et al., 2021, 2020). On site-city interaction, Lu et al. (2018) proposed a nonlinear numerical coupling in SEM. An alternative, more efficient procedure suggests a coupling method for physic-based large-scale numerical wave propagation solution. Bielak et al. (2003), proposed a domain reduction method (DRM) to reduce the large computational costs of an end-to-end simulation and to apply to an equivalent force field calculated from the solution of a simpler larger domain model to a smaller local domain. This two-step approach consists of applying a weak coupling between two models, offering a simple resolution of wave propagation from fault to structure with an acceptable computational cost (e.g. Jeremic et al., 2009; Russo et al., 2017; Abell et al., 2018; Luo et al., 2019; Zhang et al., 2020; McCallen et al., 2021; Wang et al., 2021; Korres et al., 2022). Most recently, this approach was adopted for SSI analysis by Wang et al. (2021) using potential wave formulation to create a spatially varying inclined seismic wavefield and by Zhang et al. (2020) using SEM and FEM coupling.

In this article, the DRM methodology for SEM-FEM coupling, to perform a SSI analysis from the fault to the structure is proposed and verified, offering easier implementation and performance compared to the strong coupling approach. The latter, on the other hand, consists in simultaneously solving and communicating the two divided problems at each time steps (Brun et al., 2021; Zuchowski et al., 2018).

In the frame of the French research project SINAPS@ (Earthquake and Nuclear Installations: Ensuring and Sustaining Safety (Berge-Thierry et al., 2017), we have applied the proposed SEM-FEM coupling on the CEA (French Alternative Energies and Atomic Energy Commission) Cadarache site, located in the South-Eastern France. We have also compared the SEM-FEM coupling analysis to the Full FEM analysis for SSI (one-step

approach for SSI analysis using FEM Saez et al., 2011) and Free Field (FF). Finally, the choice of the input motion implementation for the Full FEM analysis is discussed in a sensitivity study.

2. DOMAIN REDUCTION METHOD APPLIED FOR THE SEM-FEM DOMAINS COUPLING

The DRM method (Bielak et al., 2003) proposes a two-step analysis to solve the global problem of seismic wave propagation from the source to the site surface, which are often several tens or even hundreds of kilometers apart. Thus, the method divides the initial problem into two simpler ones (Figure 1). The first problem simulates the effects of the seismic source and wave propagation with a model that includes the source and the site domain by removing local effects, such as the site effect and the SSI (Ω_{SEM} in Figure 1). This domain is modeled using SEM3D, a 3D High-Performance SEM code for non-linear seismic wave propagation (CEA et al., 2017). The second problem (Ω_{FEM} in Figure 1) models the local site effects by considering a set of equivalent forces, derived from the first step, and imposed on the edges of the subdomain. This domain is modeled using Cast3M, a FEM code for structural and fluid mechanics (CEA, 2021). The discretized dynamic equilibrium equation of the wave propagation problem in the global assembled domain $\Omega = \Omega_{FEM} + \Omega_{SEM}$ is written in Equation *(1)*, where $\ddot{u}$ and u are the acceleration and displacement vectors, respectively, and F is the external loading vector. The matrices M and K represent the mass and stiffness matrices, respectively. The indices i, b and e denote the interior, the boundary and the exterior of the domain defined as the suffix.

$$\begin{bmatrix} M_{ii}^{\Omega_{FEM}} & M_{ib}^{\Omega_{FEM}} & 0 \\ M_{bi}^{\Omega_{FEM}} & M_{bb}^{\Omega_{FEM}} + M_{bb}^{\Omega_{SEM}} & M_{be}^{\Omega_{SEM}} \\ 0 & M_{eb}^{\Omega_{SEM}} & M_{ee}^{\Omega_{SEM}} \end{bmatrix} \begin{bmatrix} \ddot{u}_i^{\Omega_{FEM}} \\ \ddot{u}_b^{\Gamma} \\ \ddot{u}_e^{\Omega_{SEM}} \end{bmatrix} + \begin{bmatrix} K_{ii}^{\Omega_{FEM}} & K_{ib}^{\Omega_{FEM}} & 0 \\ K_{bi}^{\Omega_{FEM}} & K_{bb}^{\Omega_{FEM}} + K_{bb}^{\Omega_{SEM}} & K_{be}^{\Omega_{SEM}} \\ 0 & K_{eb}^{\Omega_{SEM}} & K_{ee}^{\Omega_{SEM}} \end{bmatrix} \begin{bmatrix} u_i^{\Omega_{FEM}} \\ u_b^{\Gamma} \\ u_e^{\Omega_{SEM}} \end{bmatrix} = \begin{bmatrix} 0 \\ 0 \\ F_e \end{bmatrix} \quad (1)$$

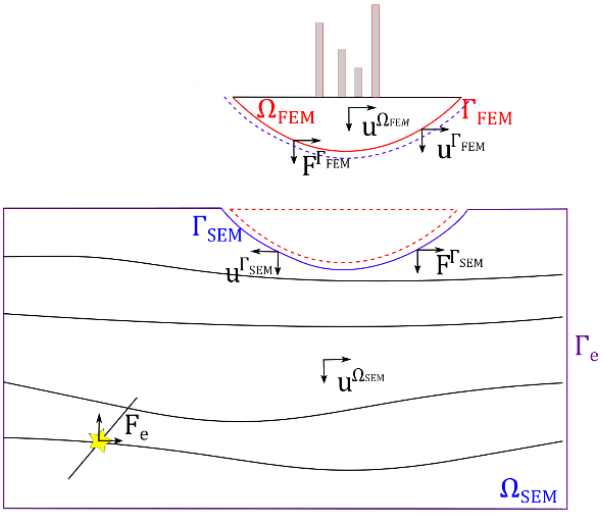

Figure 1. Overview of the forces and displacements applied to the boundaries of the domains Ω_{SEM} and Ω_{FEM}.

In equation *(1)*, the displacement is continuous at the boundaries Γ_{SEM} and Γ_{FEM} giving $u^{\Gamma} = u^{\Gamma SEM} = u^{\Gamma FEM}$ and $\ddot{u}^{\Gamma} = \ddot{u}^{\Gamma SEM} = \ddot{u}^{\Gamma FEM}$. Hence, Γ refers to the boundaries Γ_{SEM} or Γ_{FEM}. Moreover, according to the reciprocity theorem, the loading Γ_{FEM} is equal to the opposite of the forces calculated at Γ_{SEM} $F^{\Gamma FEM} + F^{\Gamma SEM} = 0$.

In order to solve the wave propagation problem in Ω_{FEM}, taking into account the effect of Ω_{SEM}, the equivalent force F_{eff} is calculated from the solution of the wave propagation in Ω_{SEM} as written in Equation *(2)*. For sake of simplicity the full demonstration is not developed and readers are are invited to refer to the paper of Bielak et al., (2003) for a step by step solution.

$$F_{eff} = \begin{cases} 0 \\ -M_{be}^{\Omega_{SEM}} \ddot{u}_e^{\Omega_{SEM}} - K_{be}^{\Omega_{SEM}} u_e^{\Omega_{SEM}} \\ M_{eb}^{\Omega_{SEM}} \ddot{u}_b^{\Gamma} + K_{eb}^{\Omega_{SEM}} u_b^{\Gamma} \end{cases} \quad (2)$$

We can summarize the proposed coupling procedures in two steps:

- The first step consists of solving the wave propagation problem in SEM3D from the fault to the free surface in Ω_{SEM}. The corresponding model considers the soil heterogeneity in x, y and z directions, the topography of the medium, and the fault rupture mechanism. The displacements and constraints time histories at the boundary Γ are logged.
- In the second step, the equivalent force F_{eff} hence calculated, according to Equation *(2)*, is provided as input loading for the wave propagation problem in Ω_{FEM}. The corresponding model considers the soil heterogeneous in the vertical direction z and the constructed surface to take into account the SSI effect.

In this paper, the proposed coupling is restrained to the linear elastic regime.

3. VERIFICATIONOF THE PROPOSED SEM3D-CAST3M COUPLING

To be able to rely on the solution provided by the coupled computer codes, the quality of the solution needs to be evaluated. Among developers, verification and validation procedures are used to benchmark the solution with analytical or experimental outcomes (Schwer, 2009). In the field of soil dynamics, the analytical solution is not available especially for elasto-plastic or nonlinear behavior of the soil and the experimental results are hard to obtain. Hence, the V & V procedures are complicated to apply. However, there is also counter verification, where the solution is benchmarked by using the results of a verified code or from a very fine discretization. This section aims at verifying the employed procedure of coupling between both codes SEM3D and Cast3M, both validated codes in soil and structural dynamics (Gatti, 2017; Touhami et al., 2022, 2022; Wang and Rambach, 2013),

Example 1: Counter verification of the coupling procedure with either Cast3M and SEM3D solutions

In order to verify the implementation of the DRM, the first example shows the comparison between a Full FEM analysis (analysis for which the solution is calculated in the domain Ω) using the FEM code Cast3M and a FEM-FEM analysis (the first FEM analysis solves the wave propagation in Ω and the second one in Ω_{FEM}, Figure 2) using the same FEM code Cast3M. A homogeneous soil with a bulk density $\rho = 2000\ \mathrm{kg/m^3}$, a shear wave velocity $v_s = 300\ \mathrm{m/s}$ and a body wave velocity $v_p = 700\ \mathrm{m/s}$, is modeled. The soil domain Ω has larger dimensions of $10\mathrm{m} \times 10\mathrm{m} \times 10\mathrm{m}$. The domain Ω_{FEM} is totally embedded in the domain Ω, with which it shares five boundary surfaces, and has a smaller dimension of $1\mathrm{m} \times 1\mathrm{m} \times 1\mathrm{m}$ (Figure 2). A Ricker-type signal is applied as a seismic input motion with a frequency equal to 5 Hz. The same time step $\Delta t = 0.01$ s is adopted for Full FEM and FEM-FEM implicit analyses. When comparing the acceleration time histories registered at the center of the top ground surface for both analyses (Figure 3), a match in time and frequency domains is obtained with a difference in the peak ground acceleration (PGA) of less than 1%.

This same example is repeated to compare the Full SEM and the SEM-FEM coupling results. The input motion for the Full SEM model in SEM3D is a sinusoidal point source of frequency equal to 5 Hz. When comparing the acceleration time histories registered at the center of the top ground surface for both analyses (Figure 4), we obtain a difference in PGA less than 8%, which may be due to the employed interpolation at the shared surfaces nodes and the employed boundary conditions (BC). In fact, contrary to the previous Full FEM model, the Full SEM model mesh does not conform to the mesh of the reduced FEM model. In addition, the soil boundaries (lateral and at the base of the domain) damping used in Cast3M corresponds to a Lysmer-type absorbing layer (Lysmer and Kuhlemeyer, 1969; Lysmer et al., 1975), whereas the one used in SEM3D is a Perfectly Matched Layer (PML)-type absorbing layer applied(Festa and Vilotte, 2005). Finally, a Rayleigh numerical damping is used in Cast3M according to (Clough and Penzien, 2003; Hughes, 1987), with a damping matrix in the form $C = \alpha M + \beta K$. The Rayleigh damping is related to the inverse of the quality factor, according to the approximate relation $Q_s = Q_p = v_s/10$, such that $Q^{-1} \approx 2\xi \approx \alpha/\omega + \beta\omega$ where $\omega = 2\pi f$ is the pulsation and ξ the damping factor (Semblat, 1997). In SEM3D on the other hand, no damping is applied.

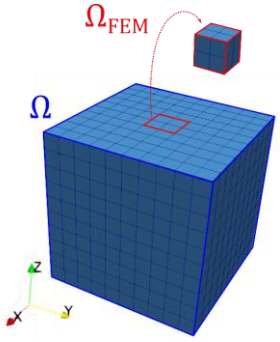

Figure 2 Mesh of the Full FEM domain Ω and the reduced domain Ω_{FEM}.

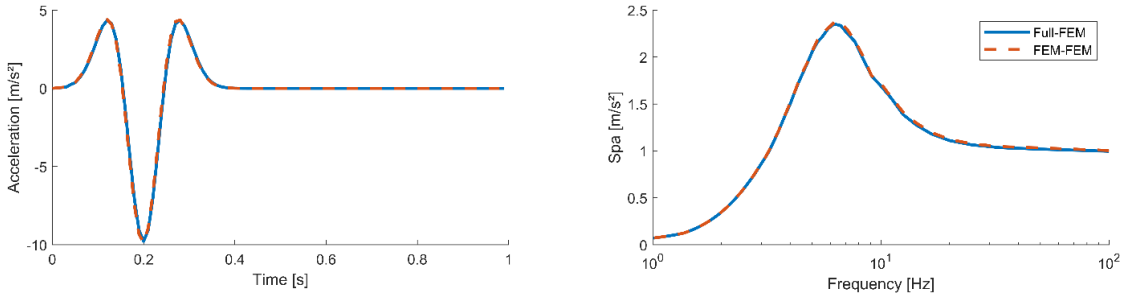

(a) (b)

Figure 3 Comparaison of the time history accelerations (a) and spectral responses (b) between Full FEM and FEM-FEM coupling analyses.

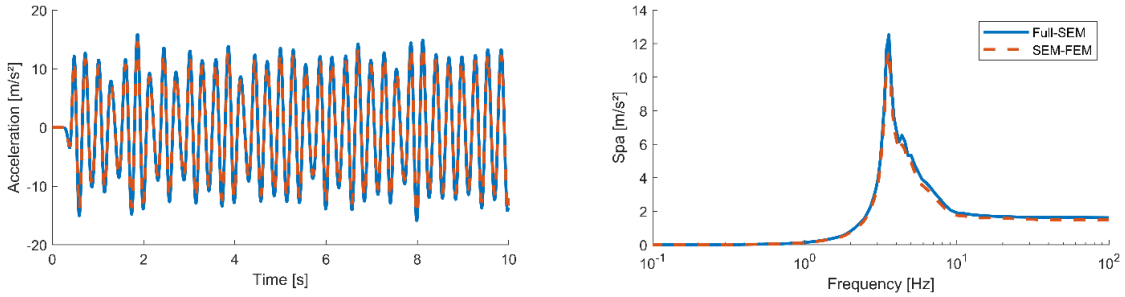

(a) (b)

Figure 4 Comparaison of the time history accelerations (a) and spectral responses (b) between Full SEM and SEM-FEM coupling analyses.

Example 2: Counter verification of coupling procedure for PRENOLIN case study

In order to verify the soil response solution, this example investigates the case study P1 in Régnier et al., 2016. A homogeneous soil cubic medium of $10\text{m} \times 10\text{m} \times 10\text{m}$ is modeled with a density of $\rho = 1800\ \text{kg/m}^3$, a shear wave velocity of $v_s = 300\ \text{m/s}$ and a body wave velocity of $v_p = 700\ \text{m/s}$. The solution is computed for a FF assumption.

In order to quantify the differences between the results at each node of the top ground surface for the coupling method and SEM method, Goodness of Fit (GoF) scores are calculated as proposed by Anderson, (2004). Figure 5-b shows the mapping of GoF scores at the top ground surface of Ω_{FEM}, where the results are compared according to 9 criteria with a scoring scale ranging from 0 (null fit) to 10 (excellent fit): Arias duration ($C1$), energy duration ($C2$), Arias intensity ($C3$), energy integral ($C4$), peak ground acceleration ($C5$), peak ground velocity ($C6$), peak ground displacement ($C7$), response spectrum ($C8$), Fourier spectrum ($C9$), over the band frequency 0.1-20Hz, and cross correlation ratio ($C10$). The lowest score is obtained for the Fourier spectrum $C9 = 8.1$, which corresponds however to an excellent fit according to Anderson, (2004). Hence, the coupling procedure is considered as verified.

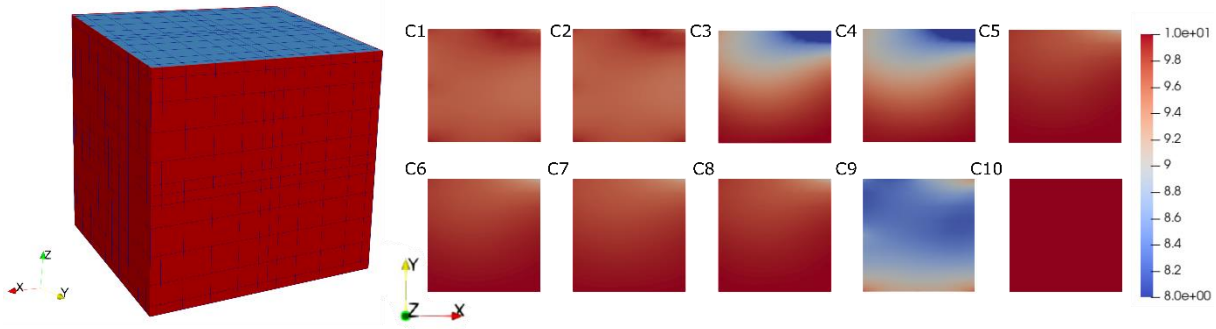

(a) (b)

Figure 5 Mesh of the FEM model (a), mapping of the Goodness of Fit scores at the top ground surface of Ω_{FEM} (b).

4. APPLICATION TO THE CADARACHE SITE SIMULATION

The Cadarache site is a CEA center located in the South-Eastern France, with several basic nuclear facilities. It has been chosen for this study, as it is a well-instrumented site with many data on the 3D geological model, including the Middle Durance Fault, the sedimentary basin and the seismic activity. A careful seismic hazard evaluation exists for this zone due to safety requirements for the existing nuclear facilities and the proper functioning of their equipment against earthquakes.

In this study, the SEM3D model is used to solve the wave propagation from the fault to the free surface and to provide the displacement field at each node of the interface with the Cast3M model. In a second step, the force fields are calculated, according to the DRM (Equation (2). The wave propagation is, hence, calculated from the near soil to the structure by solving the dynamic equilibrium equation of the assembly.

This procedure allows for the SSI effect while providing more accurate estimation of site effects, including the topography, the spatial variation of soil properties, and the sedimentary basin geometry, due to the variable force field loading.

Hereafter, we present details of the SEM3D and Cast3M models for the Cadarache site and we discuss the impact of the way to impose the input motion for the Full FEM analysis.

SEM3D MODEL DESCRIPTION

The numerical earthquake model is implemented in SEM3D. Using the same code, Castro-Cruz et al. (2021) have proposed a hybrid approximation between a physic-based simulation and the Empirical Green function method for the Cadarache site. The study in this paper uses the same geological and source information. The model mesh for the Cadarache region contains ca. 5.9 million linear hexahedral elements for a total of 5.9 billion DOFs. PML absorbing boundary conditions are applied at the model boundaries.

The mesh solves with high accuracy the wave-propagation problem up to a maximum frequency of $8Hz$. The elements have a minimal length of $105.8m$ and $45.7m$ inside the basin. Additionally, by using transition elements (Figure 6), with irregular hexahedrons, the elements size is larger at deeper parts where soil mechanical properties are stronger than those for the shallow layers.

Figure 7 presents the kinematic source introduced in the model, as a double couple mechanism by displacement imposition. This source starts around the center of the fault, and the rupture process takes around $3.8s$. The maximal slip in the rupture reaches 1.1m, and the maximal released seismic moment by second is $6 \times 10^{17}\ Nm/s$. The total seismic moment is equal to 1.04×10^{18} ($M_w = 6.0$), which is the same magnitude as other studies in the area (e.g. Dujardin et al., 2020), and corresponds to the maximal reported magnitude in the instrument database of France (Baroux et al., 2003).

The Cadarache sedimentary basin model comes from the preliminary works of Guyonnet-Benaize, (2011), and has been regularly updated by the Commissariat à l'énergie atomique et aux énergies alternatives (CEA) by integrating the new data available. The basin model is constituted from thousands of boreholes investigations and numerous H/V measurements. Further details are found in Perron et al., (2018). Castro-Cruz et al. (2021) present the validation and a deeper description of the implemented geology in this model which is also used in this study. The integration between SEM and FEM allows making specific analyses on the SEM simulation. Using SEM, we predict the results at all the mesh nodes in FEM (Figure 8). The SEM model is much bigger, allowing for regional analysis, and the FEM model contributes to a more refined structural analysis.

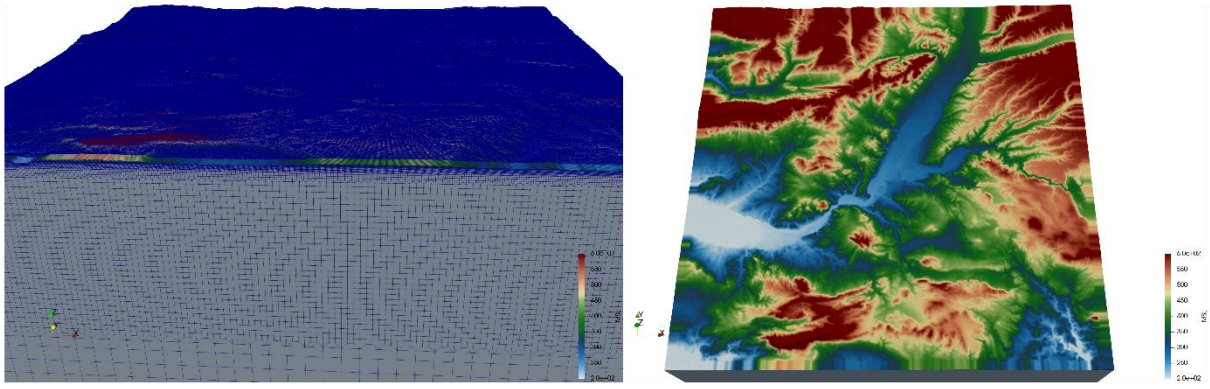

(a) *(b)*

Figure 6 Mesh of the Cadarache site in SEM3D (a) and mapping of the geological model (b).

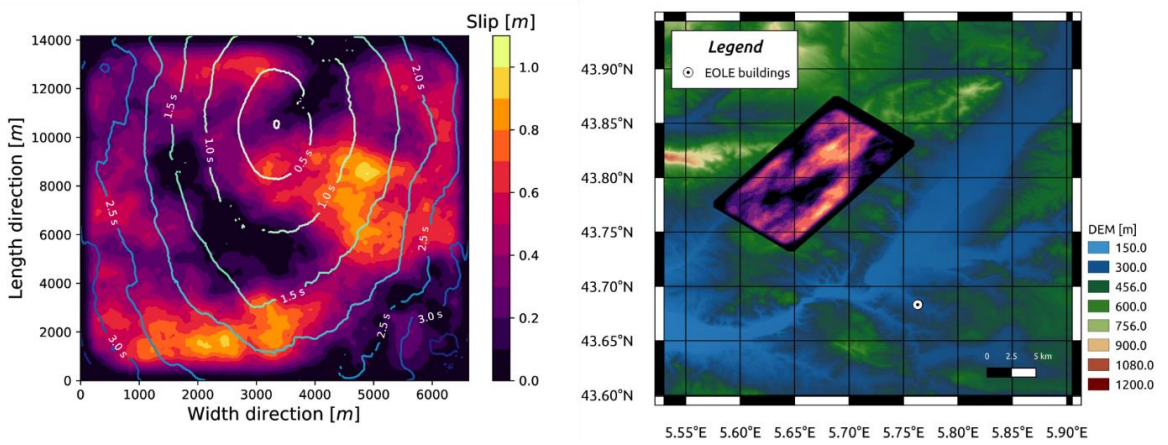

Figure 7 Seismic source for an $M_w = 6$earthquake, outline of the static slip distribution (a), Map of the region of interest, including the extended fault (b).

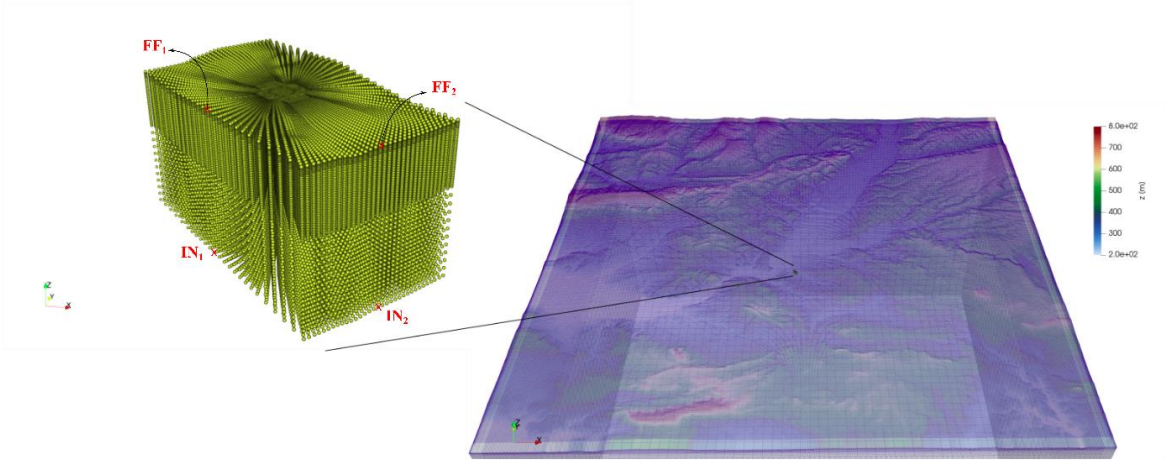

Figure 8 Zoom on the receivers at which the results are predicted in the SEM3D model

CAST3M MODEL DESCRIPTION

The soil model

This study performs the coupling method using Cast3M. The soil domain modeled in Cast3M has a dimension of $250\text{m} \times 500\text{m} \times 250\text{m}$ in $\boldsymbol{x}, \boldsymbol{y}$ and $\boldsymbol{z}$ directions respectively and is located inside the basin region (Figure 9). The soil domain is rotated 45° around the $\boldsymbol{z}$ axis to match the corresponding configuration in the Cadarache site (Figure 9-a and b). The model uses a soil stratigraphy in agreement with the geological description of Cadarache site (Appendix A), with a horizontal homogenization of the soil stratigraphy to satisfy the vertical propagation assumption considered in the solution of the dynamic equilibrium equation in Cast3M. The adopted stratigraphy considers thin layers of $\Delta h \leq 5$ m in the basin.

To realize SSI analysis higher frequency resolution is essential for engineering applications (Baker et al., 2014). The objective of the study herein is to extend the resolution to frequencies relevant to structures. Moreover, higher frequencies are observed as a result of wave scattering due to heterogeneous velocities in soil (Imperatori and Mai, 2015; Takemura et al., 2015). Hence the maximum frequency of interest in this study is set to $f = 20$ Hz. The soil model is meshed by hexahedral elements with quadratic interpolation for the displacement DOFs. The minimum number of elements is defined by the analytical relation $pfh/2v_s$, where h is the thickness of the soil layer and $p = 10$ is the minimum number of points per wavelength and v_s is the shear wave velocity of the soil layer (Fares, 2018). At the mesh boundaries, the model has a Lysmer-like absorbing condition to ensure the attenuation of wave propagating towards infinity. The Newmark integration scheme is adopted for the time resolution of the dynamic equilibrium. A Rayleigh damping model is used, to introduce frequency dependent attenuation, and is calibrated on frequencies $f_1 = 2$ Hz and $f_2 = 20$ Hz. The damping matrix is estimated by: $C = \alpha M + \beta K$ where $\alpha = 2\zeta\omega_1\omega_2/(\omega_1 + \omega_2)$, $\beta = 2\zeta/(\omega_1 + \omega_2)$ and ω_1 and ω_2 are the angular frequencies associated with the frequencies f_1 and f_2 respectively. The simulations are performed in the time domain assuming linear behavior

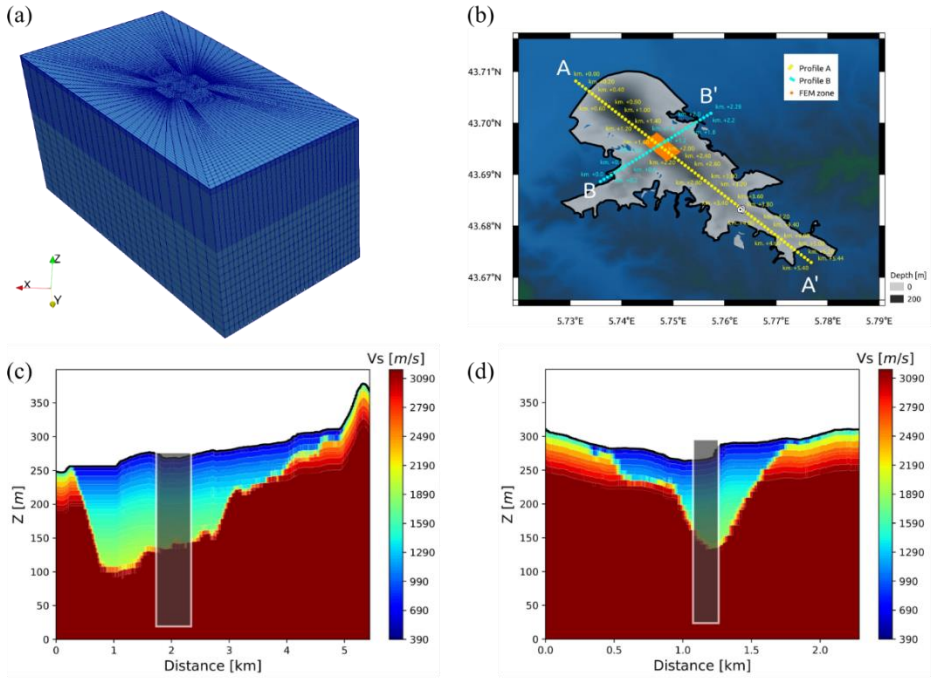

Figure 9 The soil mesh (a), the basin site (b), section AA' (c) and BB' (d) of the basin

for both the structure and the soil with a time step equal to $\Delta t = 1/(4 \times f_c) = 0.00125$ s, where f_c represents the signal cutoff frequency.

The structure model

A virtual structure - corresponding to a simplified Pressurized Water Reactor (PWR)-type building - is positioned on the Cadarache site. The used FEM model represents the detailed structure with median properties and it incorporates all the buildings of the nuclear island, i.e. the containment, the internal structures, as well as the backup buildings and the common basement.

The structure has two planes of symmetry along $(\boldsymbol{Oxz})$ and $(\boldsymbol{Oyz})$ (Figure 10). It is composed of a 3 m thick foundation with dimensions 70m × 100m × 65m and is modeled by 2D shell elements: the dome by 3-node shell elements (COQ3), the walls and floors by 4-node shell elements (COQ4) and the invert by 8-node shell elements (COQ8). The mechanical characteristics of the material (homogenized) composing the structure are presented in Appendix A. The frequency of the first natural mode in bending the structure is 3.8 Hz. The structure is connected to the ground by a rigid link at each node.

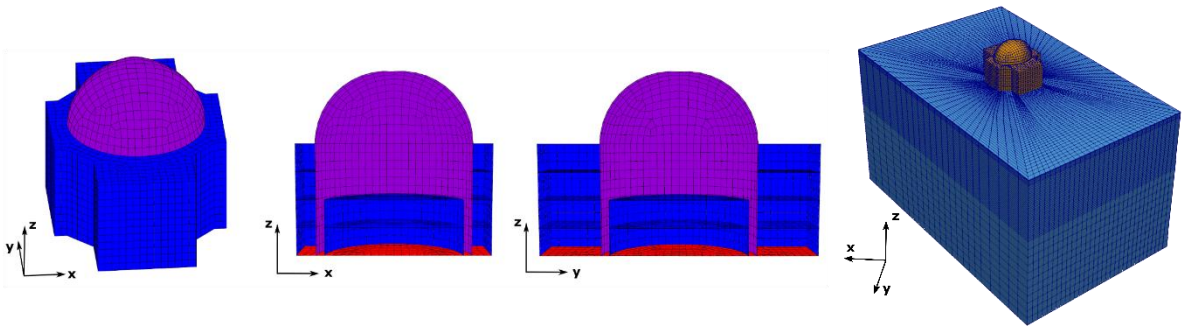

(a) *(b)* *(c)* *(d)*

Figure 10 The simplified reactor building mesh: (a) 3D view, (b) plan view $(\boldsymbol{Oxz})$ and (c) plan view $(\boldsymbol{Oyz})$ and the SSI model mesh (d).

Investigation on input motions

The choice of the input signal is critical for the accuracy of the Full FEM analysis in a nearfield domain. In the context of SEM-FEM coupling, the method employs a spatially variable field at the reduced FEM domain boundaries. However, in the Full FEM analysis, the method uses a uniform plane wave loading according to the

employed absorbing boundary condition (Lysmer and Kuhlemeyer, 1969). To generate this input field for the full FEM analysis, we perform a deconvolution process from a FF input signal and a convolution process from an inside bedrock (IN) input signal. The deconvolution is solved in the time domain with a transition to the frequency domain by the computation of the transfer functions. It consists of calculating over a column soil profile the dynamic response of each node to an impulsive horizontal input force applied at the bottom according to the Rayleigh damping model. The convolution process is identical to the deconvolution one, but the first one predicts the FF starting with a bedrock record and the other predicts the bedrock motion from a FF record. For simplicity, the term deconvolution is adopted hereafter for both processes unless specified.

In this study, 4 different input motions are investigated: two registered at the FF (FF_1 and FF_2) and two others at the corresponding bedrock (IN_1 and IN_2) (Figure 8 and Figure 11). Figure 12 shows a comparison between the deconvolution and the Full SEM results in terms of normalized acceleration time histories in the soil profile for different depths. The normalization is done according to the maximum between the maximum of absolute accelerations $max|a_{z=h}^{FullSEM}|$ and $max|a_{z=h}^{deconvolution}|$ at each depth h. A quantification of the differences is calculated in Table 1 computing the mean GoF coefficients at each node n in the soil profile between Full SEM and deconvolution time history acceleration results for $\boldsymbol{x}$, $\boldsymbol{y}$ and $\boldsymbol{z}$ directions ($\mu_{x,y,z}(C1) = \mu$)). The obtained results for the deconvolution of the FF input signals show an excellent score for all coefficients and a good score only for the Fourier spectrum coefficient $C9$. However, the results obtained for the convolution of bedrock input motions show less accuracy to reproduce the FF signal and register good results for all coefficients and very poor results for the Arias intensity and Fourier spectrum coefficients $C8$ and $C9$ respectively. This result may be due to the content of the FF input motions impacted by the wave propagation in the stratified soil profile. On the other hand, the convolution of the bedrock input motions predict amplified FF signals.

*Table 1 Mean GoF coefficients on results at each node in the soil profile between Full SEM and deconvolution / convolution time history acceleration results for **x**, **y** and **z** directions.*

	$\mu_{x,y,z}(C1)$	$\mu_{x,y,z}(C2)$	$\mu_{x,y,z}(C3)$	$\mu_{x,y,z}(C4)$	$\mu_{x,y,z}(C5)$	$\mu_{x,y,z}(C6)$	$\mu_{x,y,z}(C7)$	$\mu_{x,y,z}(C8)$	$\mu_{x,y,z}(C9)$	$\mu_{x,y,z}(C10)$
FF_1	9.17	9.80	9.76	9.95	9.93	9.98	10.00	9.72	6.50	9.99
IN_1	7.15	7.09	0.47	3.80	5.90	9.25	7.08	6.09	0.43	9.15
FF_2	9.14	9.73	9.06	9.91	9.67	9.97	10.00	9.50	5.66	9.99
IN_2	7.45	7.48	0.77	4.50	7.65	9.58	5.54	7.45	0.43	9.44

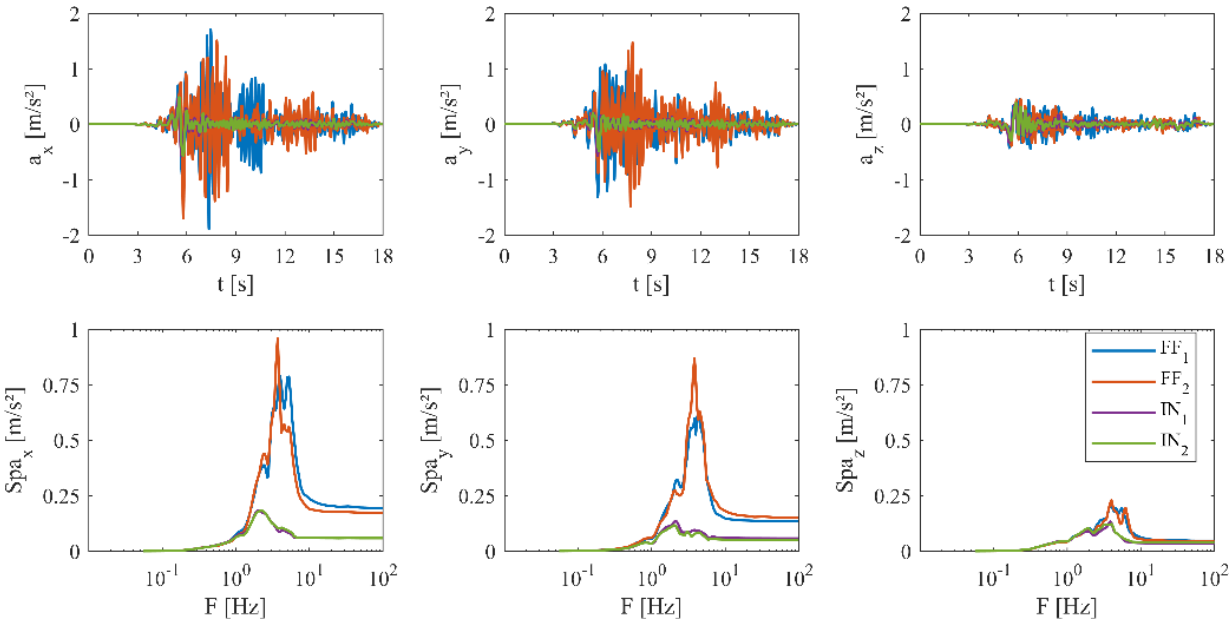

*Figure 11 Time history accelerations of the studied input signals (top) and their corresponding spectral responses (bottom) in **x**, **y** and **z** directions.*

FF_1 IN_1 FF_2 IN_2

*Figure 12 Comparison of the normalized time history accelerations along the soil profile depths for the Full SEM and the deconvolution / convolution results in **x**, **y** and **z** direction from top to bottom respectively.*

FREE FIELD ANALYSIS

This section presents the study of the choice in the input signal considering the site effects related to the topography, the spatial heterogeneity of the mechanical properties of the soil, and the surface waves. For this purpose, the Cadarache site is modeled in a 3D soil domain, as described previously. Contrary to the deconvolution procedure, the Full FEM and SEM-FEM analyses solve the dynamic equilibrium equation for the wave propagation in the 3D soil domain. Figure 13 and Figure 14 show a comparison between the mappings of the spectral responses of the soil surface along with the free surface lines AA' and BB' respectively (Appendix B, Figure B-1) for the SEM-FEM, and Full FEM analyses considering the input motions FF_1,IN_1, $FF_2$and IN_2.

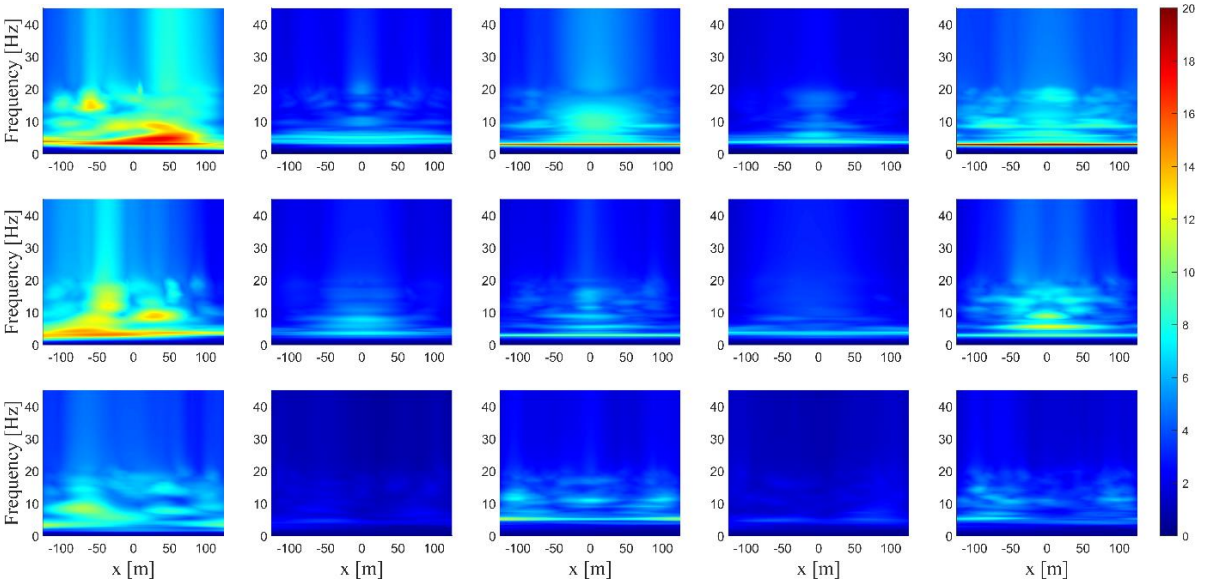

SEM-FEM FF_1 IN_1 FF_2 IN_2

Figure 13 Mapping of the spectral responses of the soil surface along the free surface lines AA' for the SEM-FEM coupling and Full FEM analyses considering the input motions F_1,IN_1, FF_2 and IN_2 .

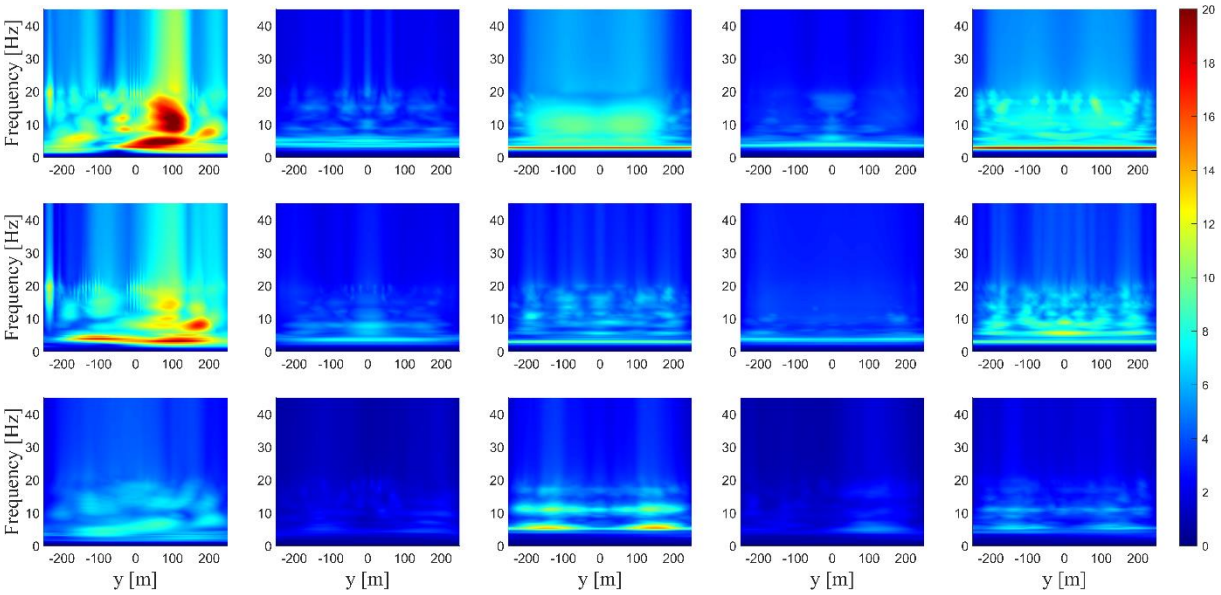

Figure 14 Mapping of the spectral responses of the soil surface along the free surface lines BB' for the SEM-FEM coupling and Full FEM analyses considering the input motions FF_1, IN_1, FF_2 and IN_2 .

The Full FEM analysis results underestimate the soil response, compared to SEM-FEM analysis. In fact, the SEM-FEM analysis allows the surface wave propagation due to the spatially variable input field. Hence, it allows a better estimation of the site effects in the soil. Although the FF input signals lead to satisfying results for the deconvolution analysis, in a Full FEM 3D wave propagation approach, the bedrock input signals perform better. According to the results obtained for input motions IN_1 and IN_2in Figure 13 and Figure 14, the predominant frequency and its associated amplification correspond to the solution in SEM-FEM coupling. Whereas results obtained for input motions FF_1 and FF_2 show a slightly higher frequency with an attenuated energy.

SOIL-STRUCTURE INTERACTION

Modeling the wave propagation in a Full FEM 3D domain of reasonable size requires introducing boundary conditions chosen with care. This attention allows the reproduction of the diffracted wave field at infinity and limits the parasitic edge reflections (Snell's law) that can strongly degrade the solution. This is why it is not possible to consider Dirichlet type boundary conditions (i.e. imposed displacements), unless the boundary is moved away considerably, at the cost of significantly increased computation time and memory consumption, due to the increase in the size of the mesh and the number of associated DOFs.

In the case of SSI, it is preferable to use an absorbing boundary condition, which allows reproducing the far field solution (Hudson et al., 1994). Nevertheless, this type of boundary generally requires the structure to be moved away from the boundaries (lateral and at the base of the domain), in order to ensure a normal incidence of the waves at the edges, otherwise, the absorption conditions will be strongly degraded. Thus, the condition proposed by Lysmer and Kuhlemeyer (1969) pioneers in the study of the SSI, requires, for example, to move the boundaries away from the structure by a distance of $5 \times r$ from the center of its foundation, where r represents the radius of the equivalent circular foundation. All these limitations and conditions do not apply in the case of a SEM-FEM calculation.

Figure 15 shows a comparison of the recorded accelerations in $\boldsymbol{x}, \boldsymbol{y}$ and $\boldsymbol{z}$-directions, in terms of correlation (C_r between SSI and FF results, for the soil profiles $C_1'C_1$, $C_2'C_2$ and $C_3'C_3$ (see Appendix B, Figure B-1), for the SEM-FEM coupling and Full FEM analyses considering the input motions FF_1, IN_1, FF_2 and IN_2. The correlation C_r is calculated according to the Equation *(3)* where n is the number of time steps,$a_i$is the corresponding acceleration for the time step index i, μ_a and σ_a are the mean and standard deviation of the acceleration a, respectively (Fisher, 1992). This correlation coefficient measures the linear dependence between the acceleration responses in the SSI and FF analysis and quantifies the SSI effect in the soil. A correlation $C_r = 1$ corresponds to results in the soil unaffected by the presence of the structure.

$$C_r = \frac{1}{n-1}\sum_{i=1}^{n}\left(\frac{a_{i,FF} - \mu_{a_{FF}}}{\sigma_{a_{FF}}}\right)\left(\frac{a_{i,ISS} - \mu_{a_{ISS}}}{\sigma_{a_{ISS}}}\right) \quad (3)$$

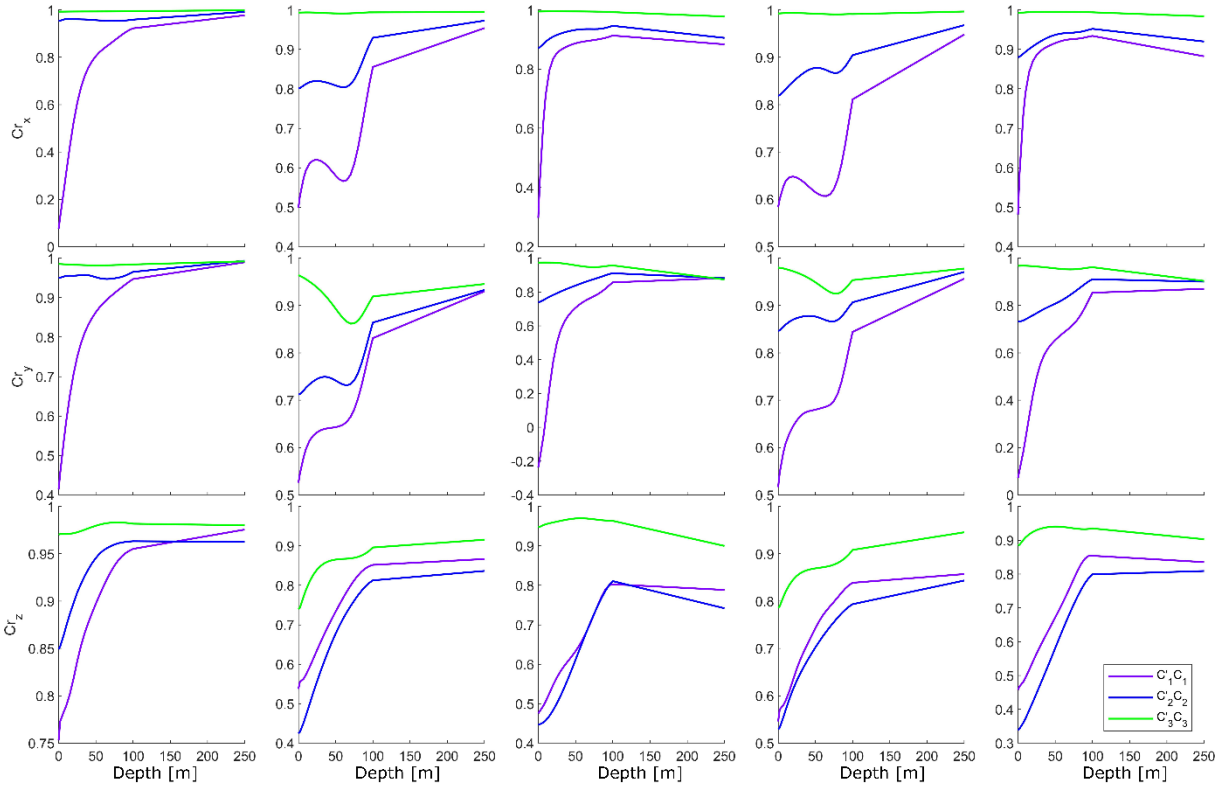

SEM-FEM FF_1 IN_1 FF_2 IN_2

Figure 15 Correlation between SSI and FF results along the line pofiles $C_1'C_1$, $C_2'C_2$ and $C_3'C_3$ for the SEM-FEM coupling and Full FEM analyses considering the input motions FF_1, IN_1, FF_2 and IN_2 .

The results confirm that the domain dimensions considered for the Full FEM SSI calculation, and suggested by Lysmer and Kuhlemeyer (1969), is sufficiently large to satisfy the vertically incident wave and the FF conditions (correlation close to 1 at the base of the model $z = 250m$ and for $C_3'C_3$). Nevertheless, it is admissible to reduce the domain size to at least 50% for a SEM-FEM SSI analysis coupled by the DRM. On the other hand, results also show the influence of the structure on the soil dynamic response, and hence the soil on the structure, depending on the analysis type and the input motion choice. In fact, for the SEM-FEM analysis, SSI is very important at the ground surface and decreases smoothly with depth. The SSI effect is observed for the Full FEM analysis with IN input motions. However, for the Full FEM analysis with FF input motions, the SSI effect is weaker in the soil and variable with depth.

The dynamic response of the Reactor Pressure Vessel (RPV) structure is examined for SEM-FEM and Full FEM analyses and presented in Figure 16. The comparison between the time history accelerations at different nodes in the structure (Appendix B, Figure B-2) for the SEM-FEM and Full FEM analyses show that the Full FEM analysis results underestimate, in most cases, the response of the structure. A shift of the structure response to lower frequencies is noticed for all Full FEM analyses. The results obtained with IN input motions tends to converge to the SEM-FEM results for higher elevations in structure and present better estimation of the structure response compared to analysis using FF input motions. Finally, the SEM-FEM analysis presents a physic-based solution for SSI analysis considering site effect and variable field input motion. The results show an amplification of the dynamic responses of the soil and the structure due to the additional site effect captured in the SEM-FEM coupling.

5. CONCLUSIONS AND DISCUSSION

In this article, the domain reduction method (DRM) is applied for the coupling between Spectral (SEM) and Finite Element (FEM) Methods, used to solve the wave propagation problem from the fault to the structure. The present study of SEM-FEM coupling leads to a more accurate solution w.r.t the SSI analysis, compared to the case of using a single (full FEM or SEM) method. The coupling method is implemented in Cast3M FEM code (CEA, 2021), and counter-verified using Full FEM (Cast3M) and Full SEM (SEM3D, CEA et al., 2017) analyses. The verification analysis of the coupling using SEM3D and CASt3M codes gives satisfactory results and suggests to use the same time steps and conforming meshes for optimal results. In addition, satisfactory results are obtained for interpolated SEM elements corresponding to the FEM elements.

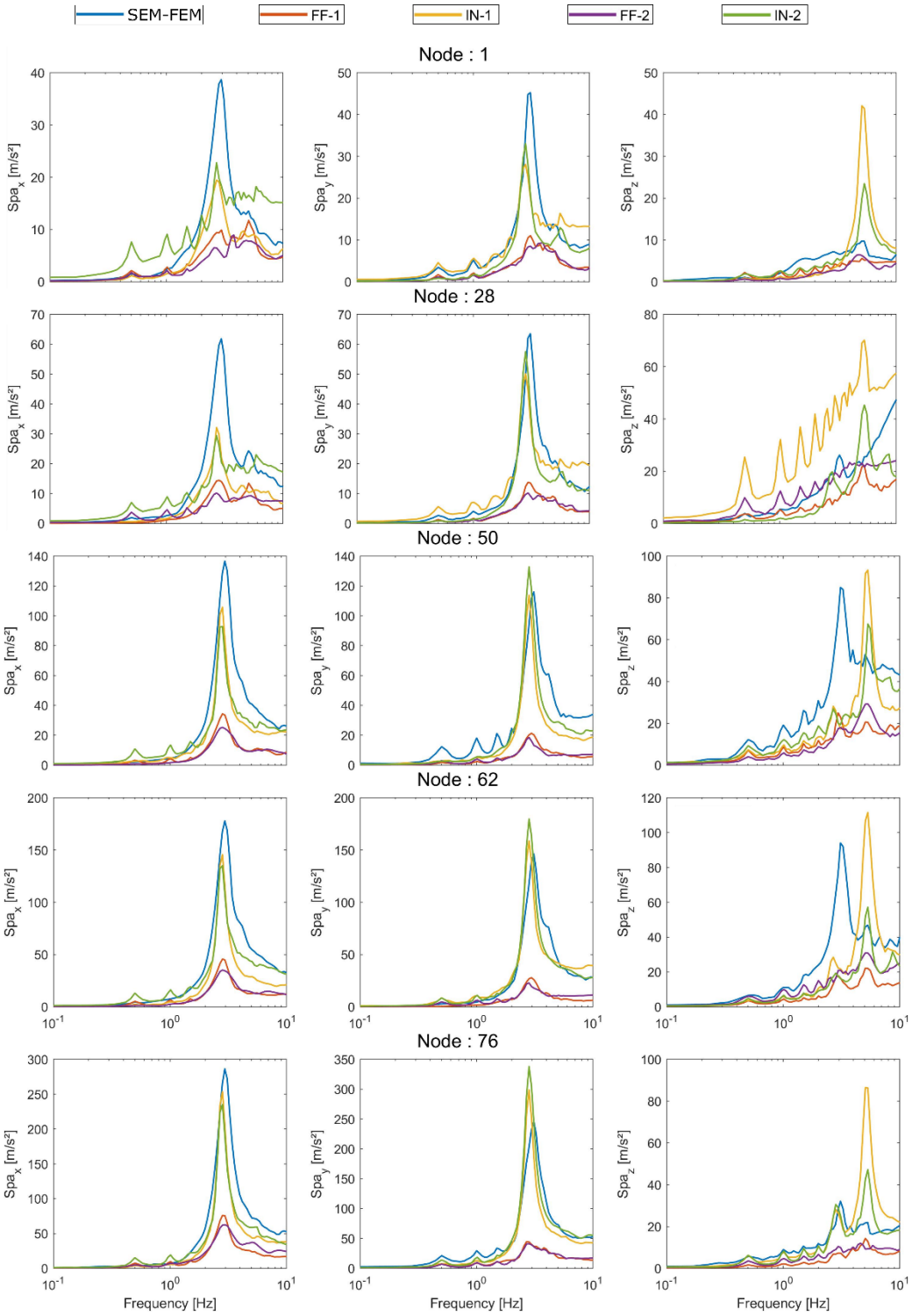

Figure 16 Comparison of the structure response spectra in $\boldsymbol{x}$, $\boldsymbol{y}$ and $\boldsymbol{z}$ directions in a SSI analysis for the SEM-FEM coupling and Full FEM analyses considering the input motions FF_1, IN_1, FF_2 and IN_2 .

The SEM-FEM coupling is adopted for the Cadarache site, locatedin the South-Eastern France. The SEM model considers the geology complexity of the site including the basin, the fault front and the topography. The FEM model considers the near soil, assumed to be horizontally stratified, and the nuclear structure corresponding to a simplified virtual PWR type building used for a SSI analysis.

A first analysis allows to compare the influence of two methods classically used to define the incident loading applied at the boundaries of the near-ground domain: (1) the approach consisting in deconvolving a free field (FF) accelerogram recorded at the ground surface of a soil column extracted from the site; (2) the approach consisting in convoluting a signal recorded at the base of a soil column (rock or other) also extracted from the site. For this

analysis, two FF input motions and two IN (inside bedrock) input motions are considered. The results obtained by these two approaches show higher accuracy for the deconvolution of the FF input motions regarding the results obtained in a Full SEM analysis. On the other hand, the results obtained by the convolution of IN input motions are amplified and can be considered as conservative in an engineering point of view.

The four wavefield calculated by the deconvolution of FF and convolution of IN input motions are nevertheless used here, for the 3D wave propagation in FF and SSI analyses. The results point out the effect of 3D wave propagation comparing to the 1D deconvolution/convolution approach. Results obtained for a FF analysis with wavefield calculated from the convolution of IN input motions show more accurate rendering of the frequency content and amplification comparing to those with wavefields calculated from the convolution of FF input motions. This result highlights the known differences between 1D and 3D wave propagation analyses. Moreover, the SEM-FEM analysis shows amplified results compared to all four Full FEM analyses as well as surface waves propagation. This is due to the additional site effect considering the topography and spatially variable field input applied at all five surface boundaries in the coupling analysis.

The SSI analysis considers a simplified PWR-type building virtually located on the CEA Cadarache site. The results show that the size of the soil domain to be considered in a SEM-FEM coupling analysis using the DRM can be reduced by 50% compared to a conventional Full FEM model size recommended by Lysmer and Kuhlemeyer (1969) to ensure an optimal absorbing boundary condition. A regular dissipation of the SSI effect as a function of depth and a concentration of these effects near the structure is observed in the cases of SEM-FEM coupling and Full FEM analyses with the IN input motions. The structure responses are amplified in SEM-FEM coupling analysis due to the additional site effect captured in this analysis.

The DRM method for SSI from the fault to the structure provides a reliable tool for a better understanding of the response of the structure in its environment. It overcomes the limitation of the SEM to model structural elements and the Full FEM to model the wave propagation from the fault, with reasonable computation resources. However, despite the advantages of the coupling some limitations of the coupled codes remains : as the limitation in the maximum frequency considered in SEM3D or the limitation of Cast3M to model local heterogeneity. On the other hand, the coupling method is only applicable in the elastic domain as it considers the superposition theorem. Nonetheless, local nonlinearities of materials can be considered in the reduced FEM domain. Further studies are necessary to define the applicability of the DRM method considering nonlinear material behavior.

Finally, the DRM's SEM-FEM coupling has proved to be a more realistic and physic-based solution for SSI analysis, taking into account the geometric and mechanical heterogeneities of the site geology in the variable input force field. However, access to geological data, seismological data, and numerical resources is mandatory for the coupling analysis and can be pretty challenging.

ACKNOWLEDGMENTS

This work lies in the framework of the SINAPS@ project funded by the French state and managed by the National Research Agency under program RNSR Future Investment bearing reference No. ANR-11-RSNR-0022-04. The SEISM Paris Saclay Research institute has supported the research reported in this paper.

Acknowledgments are given to Dr. F. Hollender, project leader, for providing the geological data for the Cadarache site and Dr F. Wang for the many interesting discussion on the topic.

REFERENCES

Abell, J.A., Orbović, N., McCallen, D.B., Jeremic, B., 2018. Earthquake soil-structure interaction of nuclear power plants, differences in response to 3-D, 3× 1-D, and 1-D excitations. Earthq. Eng. Struct. Dyn. 47, 1478–1495.

Anderson, J.G., 2004. Quantitative measure of the goodness-of-fit of synthetic seismograms.

Baker, J.W., Luco, N., Abrahamson, N.A., Maechling, P.J., Olsen, K.B., 2014. ENGINEERING USES OF PHYSICS-BASED GROUND MOTION SIMULATIONS. Stanf. Univ. 11.

Baroux, E., Pino, N.A., Valensise, G., Scotti, O., Cushing, M.E., 2003. Source parameters of the 11 June 1909, Lambesc (Provence, southeastern France) earthquake: A reappraisal based on macroseismic, seismological, and geodetic observations. J. Geophys. Res. Solid Earth 108. https://doi.org/10.1029/2002JB002348

Berge-Thierry, C., Wang, F., Feau, C., Zentner, I., Voldoire, F., Lopez-Caballero, F., Le Maoult, A., Nicolas, M., Ragueneau, F., 2017. The SINAPS@ French Research Project: first lessons of an integrated seismic risk assessment for nuclear plants safety, in: 16th World Conference on Earthquake, 16WCEE.

Bielak, J., Loukakis, K., Hisada, Y., Yoshimura, C., 2003. Domain reduction method for three-dimensional earthquake modeling in localized regions, Part I: Theory. Bull. Seismol. Soc. Am. 93, 817–824.

Boore, D.M., 1972. Finite difference methods for seismic wave propagation in heterogeneous materials. Methods Comput. Phys. 11, 1–37.

Brun, M., De Martin, F., Richart, N., 2021. Hybrid asynchronous SEM/FEM co-simulation for seismic nonlinear analysis of concrete gravity dams. Comput. Struct. 245, 106459.

Castro-Cruz, D., Gatti, F., Lopez-Caballero, F., 2021. High-fidelity broadband prediction of regional seismic response: a hybrid coupling of physics-based synthetic simulation and empirical Green functions. Nat. Hazards 108, 1997–2031. https://doi.org/10.1007/s11069-021-04766-x

CEA, 2021. Cast3M, http://www-cast3m.cea.fr/.

CEA, CentraleSupélec, IPGP, CNRS, 2017. SEM3D Ver 2017.04 Registered at French Agency for Protection of Programs (De´poˆt APP). French agency for protection of Programs (dépôt APP).

Clough, R.W., Penzien, J., 2003. Dynamics of structures, Third. ed. Computers & Structures, Berkeley, USA.

Coleman, J., Jeremic, B., Whittaker, A., 2013. Nonlinear time domain seismic soil structure interaction (SSI) analysis for nuclear facilities and draft Appendix B of ASCE 4. SMiRT-22 18–23.

Coleman, J.L., Bolisetti, C., Whittaker, A.S., 2016. Time-domain soil-structure interaction analysis of nuclear facilities. Nucl. Eng. Des. 298, 264–270. https://doi.org/10.1016/j.nucengdes.2015.08.015

Dujardin, A., Hollender, F., Causse, M., Berge-Thierry, C., Delouis, B., Foundotos, L., Ameri, G., Shible, H., 2020. Optimization of a Simulation Code Coupling Extended Source (k−2) and Empirical Green's Functions: Application to the Case of the Middle Durance Fault. Pure Appl. Geophys. 177, 2255–2279. https://doi.org/10.1007/s00024-019-02309-x

Dupros, F., De Martin, F., Foerster, E., Komatitsch, D., Roman, J., 2010. High-performance finite-element simulations of seismic wave propagation in three-dimensional nonlinear inelastic geological media. Parallel Comput. 36, 308–325.

Faccioli, E., Maggio, F., Paolucci, R., Quarteroni, A., 1997. 2D and 3D elastic wave propagation by a pseudo-spectral domain decomposition method. J. Seismol. 1, 237–251.

Fares, R., 2018. Techniques de modélisation pour la conception des bâtiments parasismiques en tenant compte de l'interaction sol-structure (thesis). Côte d'Azur.

Fares, R., Santisi d'Avila, M.P., Deschamps, A., 2019. Soil-structure interaction analysis using a 1DT-3C wave propagation model. Soil Dyn. Earthq. Eng. 120, 200–213. https://doi.org/10.1016/j.soildyn.2019.02.011

Festa, G., Vilotte, J.-P., 2005. The Newmark scheme as velocity–stress time-staggering: an efficient PML implementation for spectral element simulations of elastodynamics. Geophys. J. Int. 161, 789–812.

Fisher, R.A., 1992. Statistical Methods for Research Workers, in: Kotz, S., Johnson, N.L. (Eds.), Breakthroughs in Statistics: Methodology and Distribution, Springer Series in Statistics. Springer, New York, NY, pp. 66–70. https://doi.org/10.1007/978-1-4612-4380-9_6

Gatti, F., 2017. Analyse physics-based de scénarios sismiques «de la faille au site» : prédiction de mouvement sismique fort pour l'étude de vulnérabilité sismique de structures critiques. (phdthesis). Université Paris-Saclay ; Politecnico di Milano.

Gatti, F., Lopez-Caballero, F., Paolucci, R., Clouteau, D., 2018. Near-source effects and non-linear site response at Kashiwazaki-Kariwa Nuclear Power Plant, in the 2007 Chuetsu-Oki earthquake: evidence from surface and downhole records and 1D numerical simulations. Bull. Earthq. Eng. 16, 1105–1135. https://doi.org/10.1007/s10518-017-0255-y

Guidotti, R., Mazzieri, I., Stupazzini, M., Dagna, P., 2012. 3D numerical simulation of the site-city interaction during the 22 February 2011 MW 6.2 Christchurch earthquake, in: 15th World Conference of Earthquake Engineering.

Gupta, O., Lacoste, A.C., 2006. Prise en compte du risque sismique à la conception des ouvrages de génie civil d'installations nucléaire de base à l'exception des stockages à long terme des déchets radioactifs. Guide de l'Autorité de Sûreté Nucléaire. Guide L'Autorité Sûreté Nucl.

Guyonnet-Benaize, C., 2011. Modélisation 3D multi-échelle des structures géologiques de la région de la faille de la moyenne Durance (SE France). Aix-Marseille 1.

Hudson, M., Idriss, I.M., Beikae, M., 1994. QUAD4M: a computer program to evaluate the seismic response of soil structures using finite element procedures and incorporating a compliant base. Center for Geotechnical Modeling, Department of Civil and Environmental ….

Hughes, T.J.R., 1987. The finite element method - linear static and dynamic finite element analysis. Prentice Hall Englewood Cliff 490–567.

IAEA, I.A.E.A., 2011. Guidance Document - PART 1: K-K Unit 7 R/B Structure, PHASE I, II & III (No. IAEA-EBP-SS-WA2-KARISMA-SP-002). Vienna.

IAEA, I.A.E.A., 2009. General specification for the KARISMA Benchmark Exercise (No. IAEA-EBP-SS-WA2-KARISMA-SP-0012009). Vienna.

Ichimura, T., Fujita, K., Tanaka, S., Hori, M., Lalith, M., Shizawa, Y., Kobayashi, H., 2014. Physics-Based Urban Earthquake Simulation Enhanced by 10.7 BlnDOF × 30 K Time-Step Unstructured FE Non-Linear Seismic Wave Simulation, in: SC '14: Proceedings of the International Conference for High Performance Computing, Networking, Storage and Analysis. Presented at the SC '14: Proceedings of the International Conference for High Performance Computing, Networking, Storage and Analysis, pp. 15–26. https://doi.org/10.1109/SC.2014.7

Imperatori, W., Mai, P.M., 2015. The role of topography and lateral velocity heterogeneities on near-source scattering and ground-motion variability. Geophys. J. Int. 202, 2163–2181.

Jeremic, B., Jie, G., Preisig, M., Tafazzoli, N., 2009. Time domain simulation of soil–foundation–structure interaction in non-uniform soils. Earthq. Eng. Struct. Dyn. 38, 699–718.

Komatitsch, D., Vilotte, J.-P., 1998. The spectral element method: An efficient tool to simulate the seismic response of 2D and 3D geological structures. Bull. Seismol. Soc. Am. 88, 368–392.

Korres, M., Lopez-Caballero, F., Alves Fernandes, V., Gatti, F., Zentner, I., Voldoire, F., Clouteau, D., Castro-Cruz, D., 2022. Enhanced Seismic Response Prediction of Critical Structures via 3D Regional Scale Physics-Based Earthquake Simulation. J. Earthq. Eng. 1–29.

Koufoudi, E., Cornou, C., Grange, S., Dufour, F., Imtiaz, A., 2015. Quantification of the spatially variable ground motion and its influence on the linear and non-linear structural response of a single degree of freedom. Application to the shallow sedimentary valley of Argostoli, Greece.

Lo Frano, R., Pugliese, G., Forasassi, G., 2010. Preliminary seismic analysis of an innovative near term reactor: Methodology and application. Nucl. Eng. Des. 240, 1671–1678. https://doi.org/10.1016/j.nucengdes.2010.02.034

Lu, X., Tian, Y., Wang, G., Huang, D., 2018. A numerical coupling scheme for nonlinear time history analysis of buildings on a regional scale considering site-city interaction effects. Earthq. Eng. Struct. Dyn. 47, 2708–2725. https://doi.org/10.1002/eqe.3108

Luo, C., Lou, M., Gui, G., Wang, H., 2019. A modified domain reduction method for numerical simulation of wave propagation in localized regions. Earthq. Eng. Eng. Vib. 18, 35–52.

Lysmer, J., Kuhlemeyer, R.L., 1969. Finite dynamic model for infinite media. J. Eng. Mech. Div. 95, 859–878.

Lysmer, J., Udaka, T., Tsai, C., Seed, H.B., 1975. Flush - a Computer Program for Approximate 3-D Analysis of Soil-Structure Interaction Problems (No. PB-259332; EERC-75-30). California Univ., Richmond (USA). Earthquake Engineering Research Center.

Maeda, T., Takemura, S., Furumura, T., 2017. OpenSWPC: an open-source integrated parallel simulation code for modeling seismic wave propagation in 3D heterogeneous viscoelastic media. Earth Planets Space 69, 1–20.

Manakou, M.V., Raptakis, D.G., Chávez-García, F.J., Apostolidis, P.I., Pitilakis, K.D., 2010. 3D soil structure of the Mygdonian basin for site response analysis. Soil Dyn. Earthq. Eng. 30, 1198–1211. https://doi.org/10.1016/j.soildyn.2010.04.027

McCallen, D., Petersson, A., Rodgers, A., Pitarka, A., Miah, M., Petrone, F., Sjogreen, B., Abrahamson, N., Tang, H., 2020. EQSIM—A multidisciplinary framework for fault-to-structure earthquake simulations on exascale computers part I: Computational models and workflow. Earthq. Spectra 8755293020970982. https://doi.org/10.1177/8755293020970982

McCallen, D., Petrone, F., Miah, M., Pitarka, A., Rodgers, A., Abrahamson, N., 2021. EQSIM—A multidisciplinary framework for fault-to-structure earthquake simulations on exascale computers, part II: Regional simulations of building response. Earthq. Spectra 37, 736–761.

Mercerat, E.D., Vilotte, J.P., Sánchez-Sesma, F.J., 2006. Triangular Spectral Element simulation of two-dimensional elastic wave propagation using unstructured triangular grids. Geophys. J. Int. 166, 679–698. https://doi.org/10.1111/j.1365-246X.2006.03006.x

Moczo, P., Kristek, J., Halada, L., 2004. The finite-difference method for seismologists. Introd. Comenius Univ. Bratisl.

Perron, V., Gélis, C., Froment, B., Hollender, F., Bard, P.-Y., Cultrera, G., Cushing, E.M., 2018. Can broad-band earthquake site responses be predicted by the ambient noise spectral ratio? Insight from observations at two sedimentary basins. Geophys. J. Int. 215, 1442–1454. https://doi.org/10.1093/gji/ggy355

Raptakis, D., Chávez-García, F.J., Makra, K., Pitilakis, K., 2000. Site effects at Euroseistest—I. Determination of the valley structure and confrontation of observations with 1D analysis. Soil Dyn. Earthq. Eng. 19, 1–22. https://doi.org/10.1016/S0267-7261(99)00025-1

Régnier, J., Bonilla, L.-F., Bard, P.-Y., Bertrand, E., Hollender, F., Kawase, H., Sicilia, D., Arduino, P., Amorosi, A., Asimaki, D., Boldini, D., Chen, L., Chiaradonna, A., DeMartin, F., Ebrille, M., Elgamal, A., Falcone, G., Foerster, E., Foti, S., Garini, E., Gazetas, G., Gélis, C., Ghofrani, A., Giannakou, A., Gingery, J.R., Glinsky, N., Harmon, J., Hashash, Y., Iai, S., Jeremić, B., Kramer, S., Kontoe, S., Kristek, J., Lanzo, G., Lernia, A. di, Lopez-Caballero, F., Marot, M., McAllister, G., Mercerat, E.D., Moczo, P., Montoya-Noguera, S., Musgrove, M., Nieto-Ferro, A., Pagliaroli, A., Pisanò, F., Richterova, A., Sajana, S., d'Avila, M.P.S., Shi, J., Silvestri, F., Taiebat, M., Tropeano, G., Verrucci, L., Watanabe, K., 2016. International benchmark on numerical simulations for 1D, nonlinear site response (PRENOLIN): Verification phase based on canonical cases. Bull. Seismol. Soc. Am. 106, 2112–2135. https://doi.org/10.1785/0120150284

Russo, A.D., Sica, S., Del Gaudio, S., De Matteis, R., Zollo, A., 2017. Near-source effects on the ground motion occurred at the Conza Dam site (Italy) during the 1980 Irpinia earthquake. Bull. Earthq. Eng. 15, 4009–4037.

Saez, E., Lopez Caballero, F., Modaressi-Farahmand-Razavi, A., 2011. Effect of the inelastic dynamic soil–structure interaction on the seismic vulnerability assessment. Struct. Saf. 33, 51–63. https://doi.org/10.1016/j.strusafe.2010.05.004

Santisi d'Avila, M.P., Lenti, L., 2012. Modeling strong seismic ground motion: 3D loading path vs wavefield polarization. Geophys. J. Int.

Santisi d'Avila, M.P., Lenti, L., Gobbi, S., Fares, R., 2022. Reduced T-shaped soil domain for nonlinear dynamic soil-bridge interaction analysis. Adv. Bridge Eng. 3, 9. https://doi.org/10.1186/s43251-022-00057-y

Schwer, L.E., 2009. Guide for verification and validation in computational solid mechanics.

Semblat, J.-F., 1997. Rheological Interpretation of Rayleigh Damping. J. Sound Vib. 206, 741–744. https://doi.org/10.1006/jsvi.1997.1067

Semblat, J.F., Kham, M., Parara, E., Bard, P.Y., Pitilakis, K., Makra, K., Raptakis, D., 2005. Seismic wave amplification: Basin geometry vs soil layering. Soil Dyn. Earthq. Eng., 11th International Conference on Soil Dynamics and Earthquake Engineering (ICSDEE): Part 1 25, 529–538. https://doi.org/10.1016/j.soildyn.2004.11.003

Sextos, A.G., Kappos, A.J., 2008. Evaluation of seismic response of bridges under asynchronous excitation and comparisons with Eurocode 8-2 provisions. Bull. Earthq. Eng. 7, 519. https://doi.org/10.1007/s10518-008-9090-5

Takemura, S., Furumura, T., Maeda, T., 2015. Scattering of high-frequency seismic waves caused by irregular surface topography and small-scale velocity inhomogeneity. Geophys. J. Int. 201, 459–474.

Touhami, S., Gatti, F., Lopez-Caballero, F., Cottereau, R., de Abreu Corrêa, L., Aubry, L., Clouteau, D., 2022. SEM3D: A 3D High-Fidelity Numerical Earthquake Simulator for Broadband (0–10 Hz) Seismic Response Prediction at a Regional Scale. Geosciences 12, 112. https://doi.org/10.3390/geosciences12030112

Van Nguyen, D., Kim, D., Duy Nguyen, D., 2020. Nonlinear seismic soil-structure interaction analysis of nuclear reactor building considering the effect of earthquake frequency content. Structures 26, 901–914. https://doi.org/10.1016/j.istruc.2020.05.013

Virieux, J., 1986. P-SV wave propagation in heterogeneous media: Velocity-stress finite-difference method. Geophysics 51, 889–901.

Wang, F., Feau, C., 2017. Seismic fragility curve estimation using signals generated with GMPE-Case study on the Kashiwazaki-kariwa power plant, in: SMiRT 24, Structural Mechanics in Reactor Technology. International Association for Structural Mechanics in Reactor Technology.

Wang, F., Rambach, M., 2013. Contribution to the IAEA sol-structure interaction KARISMA Benchmark.

Wang, H., Yang, H., Feng, Y., Jeremić, B., 2021. Modeling and simulation of earthquake soil structure interaction excited by inclined seismic waves. Soil Dyn. Earthq. Eng. 146, 106720.

Zhang, L., Wang, J.-T., Xu, Y.-J., He, C.-H., Zhang, C.-H., 2020. A Procedure for 3D Seismic Simulation from Rupture to Structures by Coupling SEM and FEM. Bull. Seismol. Soc. Am. 110, 1134–1148.

Zuchowski, L., Brun, M., De Martin, F., 2018. Co-simulation coupling spectral/finite elements for 3D soil/structure interaction problems. Comptes Rendus Mécanique 346, 408–422.

APPENDIX A

Tableau A-1 Mechanical properties of the structure

Module de Young $E[GPa]$	Densité $\rho[Kg/m^3]$	Coef. d'amortissement ξ	Coef. de Poisson ν
36	5000	0.07	0.2

Tableau A-2 Velocity and density model of the Cadarache site basin

$z[m]$	$v_s(z)[m/s]$	$v_p(z)[m/s]$	$\rho(z)[kg/m^3]$
$0 \leq z \leftarrow 7m$	$400 + 130z^{0.5}$	900	2100
$z \leq -7m$	$400 + 130z^{0.5}$	$1500 + 190z^{0.5}$	2100

Tableau A-3 Velocity and density model of the Cadarache bedrock

$z[m]$	$v_s(z)[m/s]$	$v_p(z)[m/s]$	$\rho(z)[kg/m^3]$
$0 \leq z \leftarrow 60m$	$1000 + 427z^{0.4}$	$2000 + 1054z^{0.3}$	2500
$-60 \leq z \leftarrow 3000m$	3200	5600	2720

Tableau A-4 Mechanical characteristics of the FEM soil profile model

n^o	$z[m]$	$h[m]$	$v_s(z)[m/s]$	$v_p(z)[m/s]$	$\rho(z)[kg/m^3]$	ν
1	2	2	583.848	900	2100	0.13668
2	7	5	743.948	2002.69	2100	0.41996
3	10	3	811.096	2100.83	2100	0.41241
4	15	5	903.488	2235.87	2100	0.40242
5	20	5	981.378	2349.71	2100	0.39435
6	25	5	1050	2450	2100	0.3875
7	30	5	1112.04	2540.67	2100	0.38151
8	35	5	1169.09	2624.06	2100	0.37617
9	40	5	1222.19	2701.67	2100	0.37134
10	45	5	1272.07	2774.56	2100	0.36693
11	50	5	1319.24	2843.5	2100	0.36286
12	55	5	1364.11	2909.08	2100	0.35907
13	60	5	1406.98	2971.73	2100	0.35554
14	65	5	1448.09	3031.83	2100	0.35222
15	70	5	1487.66	3089.65	2100	0.34909
16	75	5	1525.83	3145.45	2100	0.34614
17	80	5	1562.76	3199.41	2100	0.34333
18	85	5	1598.54	3251.71	2100	0.34066
19	90	5	1633.29	3302.5	2100	0.33811
20	95	5	1667.08	3351.89	2100	0.33567
21	100	5	1700	3400	2100	0.33333
22	250	150	3200	5600	2720	0.25758

APPENDIX B

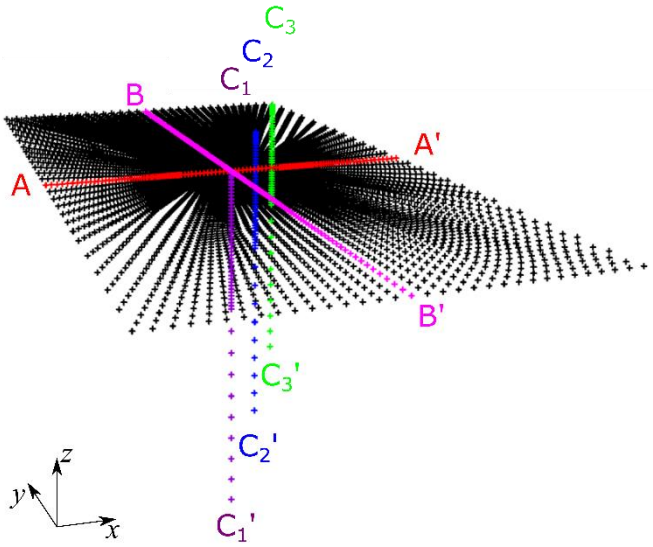

Figure B-1 Nodes lines, in the soil model, along which the results history output are evaluated

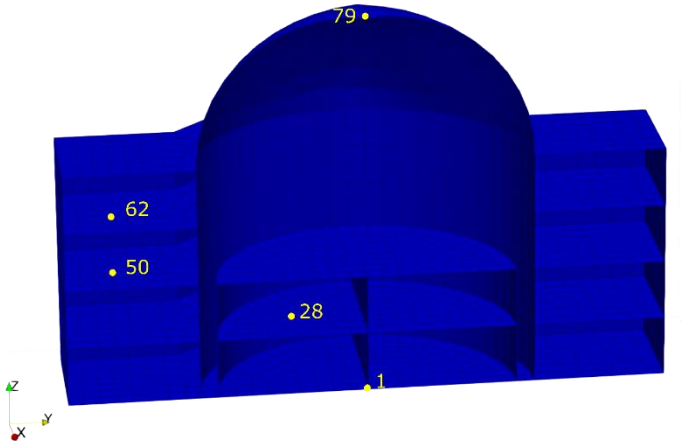

Figure B-2 Nodes in the structure model along which the results history outputs are evaluated

Table B-1 Coordinates of the observed structure nodes

Node #	*x*	*y*	*z*
1	0.0	0.0	0.0
28	10	-12	10.0
50	12	-39	20.0
62	12	-39	30.0
79	0.0	0.0	65